ACS OMEGA

http://pubs.acs.org/journal/acsodf

Article

Jet-Injection In Situ Production of PVDF/PCM Composite Fibers for Thermal Management

Mikel Duran, Artem Nikulin,* Angel Serrano, Jean-Luc Dauvergne, Yaroslav Grosu, Jalel Labidi, and Elena Palomo del Barrio

Cite This: *ACS Omega* 2023, 8, 26136−26146

Read Online

ACCESS | Metrics & More | Article Recommendations | Supporting Information

ABSTRACT: Thermal management protects against external agents and increases the lifetime and performance of the devices in which it is implemented. Because of their ability to store and release a high amount of energy at a nearly constant temperature, phase change materials (PCMs) are promising thermoregulatory materials. Thus, the manufacture of PVDF fibers containing PCMs has advantages since PVDF is already used in elements that are susceptible to thermal management as a binder in batteries or as a base material for fabrics. This work presents a simple, versatile, in situ, cost-effective, and easy-to-scale-up method to produce PVDF-based fibers containing paraffin RT-28HC for thermal management. To achieve that goal, the microfluidic approach of coaxial flows was simplified to gravity-aided laminar jet injection into a bulk fluid, where fibers were produced by the solvent extraction mechanism. With this methodology, hollow PVDF fibers and core-shell PVDF fibers containing paraffin RT-28HC have been produced. The proposed approach resulted in fibers with up to 98 J/g of latent heat, with a hierarchical porous structure. SEM study of the fiber morphology has shown that PCM is in the form of slugs along the fibers. Such PCM distribution is maintained until the first melting cycle, when molten PCM spreads within the fiber under capillary forces, which was observed by an infrared camera. Manufactured composite fibers have shown low thermal conductivity and high elasticity, which suggest their potential application as a thermal insulation material with thermal buffer properties. Leakage tests revealed outstanding retention capacity with only 3.5% mass loss after 1000 melting/crystallization cycles. Finally, tensile tests were carried out to evaluate the mechanical properties of the fibers before and after thermal cycling.

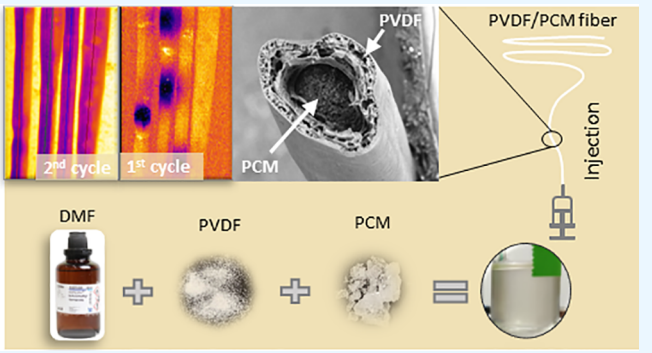

1. INTRODUCTION

Thermal management is based on transferring excess heat from one place to another. It is crucial in a variety of industrial sectors that need thermal protection against the external environment, such as aeronautics, space, buildings, food industry, textile, etc. Recently, thermal management has also become a key pillar in the development of batteries, especially for electric vehicles, as they are responsible for managing/dissipating the heat generated during the electrochemical processes occurring in the cells, allowing the battery to operate safely and efficiently.[1,2]

Due to their thermal properties, phase change materials (PCMs) with solid−liquid transitions have been extensively studied for application in thermal management devices.[3−5] The interest in these materials lies in the possibility of exploiting the high energies associated with phase changes (typically >150 J/g) that occur at a nearly constant temperature. These two characteristics make them attractive for maintaining a homogeneous temperature close to the melting point of the implemented PCM. The most studied compounds for these applications are paraffin, fatty acids, and hydrated salts. These compounds generally have melting points in the range of 10−70 °C, making them suitable for thermal management at low temperatures. Nonetheless, a severe engineering obstacle for solid−liquid PCM application is the possibility of leakages that can be driven by gravity, inertial and capillary forces.[6,7]

A variety of methods have been proposed to cope with that issue. The main idea is to encapsulate the PCMs by confining them into a closed shell or a porous matrix that prevents leaks.[8,9] As for the shape, most of the explored methods for PCMs encapsulation result in spherical shape capsules.[8] However, physico-chemical and physical methods of PCMs encapsulation can be adopted for other shape outcomes, i.e., foams or fibers.[8] Recently, the methods for encapsulation of PCMs into fibers are attracting more attention from

Received: April 6, 2023
Accepted: July 3, 2023
Published: July 12, 2023

researchers due to their high applicability for fabrics with thermal management,[10−14] thermal storage, and protection.[4,15−20] Moreover, an essential advantage of fibers is that they can further be shaped using standard and well-developed processes (weaving and knitting) that promote their sooner production at an industrial scale.

One of the approaches for PCM encapsulation into fibers is based on the coaxial jet elongation under electric field known as co-electrospinning.[21,22] This technique was applied by Chen et al.[12] to encapsulate lauric acid (LA) in PET. The resulting fibers were 710 nm in diameter with 71 J/g of latent heat. Similarly, natural soy wax was encapsulated in polyurethane (PU) by Hu and Yu[16] in the shape of fibers with an average diameter from 0.65 to 1.8 μm and up to 70 J/g of latent heat. In another two studies, the same device was employed to encapsulate capric-lauric acid and capric-palmitic acid in PET having about 55 J/g of heat of fusion,[17] as well as PEG in polyamide 6 (PA6) with a maximum latent heat of 122 J/g.[20] Emulsion electrospinning slightly simplifies the encapsulation process as it does not require a coaxial flow. Such a technique was applied by Zdraveva et al.[23] to encapsulate plant oils that serve as PCM into poly(vinyl alcohol). The PCM fibers were between 400 and 700 nm in diameter, depending on the PCM content and polymer concentration. The maximum latent heat achieved was about 97 J/g for the composite with the highest content of PCM. Despite the high storage capacity achieved by this method, the low speed of production[8] and the requirement of high voltage ranging from 12 to 20 kV[13,16] are important drawbacks of electrospinning. To overcome those limitations, a centrifugal or melt-spinning method can be used for PCM encapsulation into fibers. In the study of Yan et al.,[11] hollow polypropylene fibers were produced and later filled with PEG. With this approach, fibers of about 1000 μm in diameter and a very high PCM content on the order of 83 wt % were reached, providing up to 130 J/g of latent heat.

Looking at the previous examples, the material chosen as the fiber packaging is usually a polymeric material, mainly due to its flexibility and versatility. Among the wide variety of polymer options available, the role of polyvinylidene fluoride (PVDF) in elements that are susceptible to thermal management is particularly noteworthy. PVDF is the primary binder material used to produce composite electrodes in lithium-ion batteries. This is due to its high thermal and electrochemical stability and excellent adhesion between electrode films and collectors. PVDF is also applied as films, piping tools, sheets, or tubes.[24] In the textile sector, PVDF is usually applied for fabrics or architectural purposes like screens or filters, giving the products a long life span.[25] Song et al.[26] already reported the use of PVDF fibers and their woven textiles for passive human body cooling. They produced a hierarchically porous PVDF fiber with high mid-infrared emittance (94.5%) and opacity to solar irradiation (90.3% for near-infrared and 94.2% for visible light), which could successfully dissipate the extra heat from the human body. Given the above, the combination of PCM with PVDF seems compelling for achieving superior properties for thermal management.

This exciting combo has been little addressed in the literature to date. Nguyen et al.[13] fabricated PEG encapsulated in PVDF fibers with an average diameter of around 700 nm in nonwoven mats. The fibers contained 20 wt % of PEG with 30−35 J/g of latent heat. On the other hand, a two-step method was followed by Xiang et al.[20] for the encapsulation of paraffin. First, PVDF was dissolved in a poly(propylene carbonate) and dioctyl terephthalate mixture that afterward was extruded into ethanol to extract the solvent and form hollow fibers. In the second step, the obtained fibers were filled with paraffin up to 77 wt %, providing 80 J/g of latent heat. Finally, Haghighat et al.[27] studied various thermoregulating core-shell fibers from different polymer solutions and n-octadecane as PCM by coaxial electrospinning. Nevertheless, they concluded that PVDF was unsuitable for creating a homogenous core-shell structure. To the best of the authors' knowledge, these are the few works addressing this combination, and the proposed manufacturing procedures are complex or require multiple steps to obtain the final product. Hence, the cost efficiency and possibility of upscaling for the different synthesis methods used so far are still questionable.

Therefore, this study aims to present a simple, versatile, in situ, cost-effective, and easy-to-scale-up method to produce PVDF-based fibers intended for thermal management. The thermoregulatory properties arise from the presence of PCM (paraffin RT-28HC) within the fiber. To achieve that goal, the microfluidic approach of coaxial flows[28,29] was simplified to gravity-aided laminar jet injection into a bulk fluid, where fibers were produced by the solvent extraction mechanism. Moreover, emulsion injection was implemented for feeding the precursor materials into the system, giving place to a final process based on a chipless microfluidic approach. With this methodology, hollow PVDF fibers and core-shell PVDF fibers containing paraffin RT-28HC have been produced. The morphology and internal structure of the fibers have been thoroughly evaluated through scanning electron microscopy (SEM), whereas their thermal properties and thermal stability were evaluated by differential scanning calorimetry (DSC) and thermogravimetric analysis (TGA). Furthermore, the PCM retention capacity of the fibers was tested for 1000 thermal cycles, and the thermal response of the fibers was recorded by the IR (infrared) camera. Finally, tensile tests were carried out to evaluate the mechanical properties of the fibers before and after thermal cycling.

2. EXPERIMENTAL SECTION

2.1. Materials. In this work, two kinds of PVDF fibers were produced: pure PVDF hollow fibers, hereinafter referred to as $PVDF_{Hollow}$, and composite fibers, named $PVDF_{PCM}$. Paraffin RT-28HC with a melting point between 27 and 29 °C and latent heat of 250 J/g was supplied by Rubitherm[30] and used as a core material of the $PVDF_{PCM}$ fibers. Commercial PVDF Solef 5130 from SOLVAY was dissolved in *N*,*N*-dimethylformamide (DMF) (99.5% Pure) from EMPARTA. This solution was used as a precursor for fiber production, and tap water was utilized for the DMF extraction process.

2.2. Preparation of the Precursors. Two kinds of precursor solutions were prepared to produce $PVDF_{Hollow}$ and $PVDF_{PCM}$ fibers. The precursor for the $PVDF_{Hollow}$ fiber consisted of a 5 wt % solution of PVDF in DMF that was prepared by dissolving PVDF in DMF at 60 °C with continuous stirring. As a precursor of the $PVDF_{PCM}$ fiber, the same 5 wt % PVDF solution was used in which paraffin was added in a PVDF−paraffin mass ratio of 1:1 and emulsified by sonication in an ultrasound bath (S60H Elmasonic) at 40 °C for 30 min. No surfactant was used to stabilize the emulsion.

2.3. Production of the Fibers. In this study, the microfluidic approach of coaxial flows[28,29] was simplified to gravity-aided laminar jet injection into a bulk fluid to produce

https://doi.org/10.1021/acsomega.3c02318
ACS Omega 2023, 8, 26136−26146

fibers. A scheme of the experimental setup is shown in Figure 1. The fiber precursors were injected from a glass capillary

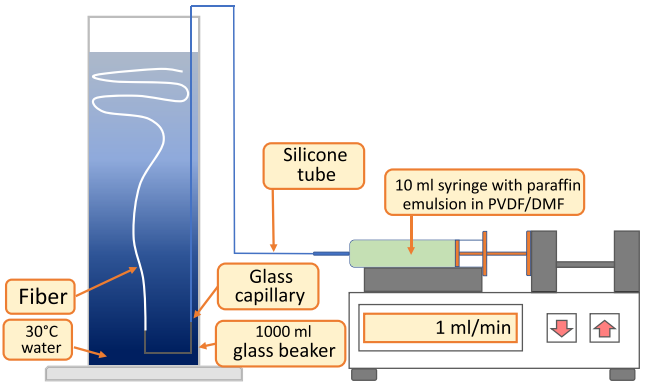

Figure 1. Scheme of the experimental setup for fiber production.

(inner diameter of 0.47 mm) into a tall glass beaker containing tap water at 30 °C. Immediately after injection, the solvent extraction process began, extracting DMF from the emulsion into the tap water. In this way, the formation of the fiber sheath takes place, trapping the paraffin inside. The injection process was started less than 10 min after emulsion preparation to avoid coagulation of the paraffin droplets. To achieve fibers with a constant diameter, a syringe pump (Pump 11 - Pico Plus Elite from HA Harvard Apparatus) was used to support the flow of precursors (at a flow rate of 0.5 mL/min) from the syringe to the glass capillary that was connected via a silicone tube. To avoid paraffin solidification during all production process, the glass beaker and the air surrounding the experimental setup were heated up to 30 °C by an electric fan heater. After the injection, the fibers were collected and stored in tap water for 24 h for the maximum extraction of DMF and then dried for 48 h at 20 °C in a fume hood. Schematic representation of the production procedure is shown in Figure 2.

2.4. Characterization. *2.4.1. Scanning Electron Microscopy.* To analyze the microstructure of the fibers, samples were imaged through a scanning electron microscope Quanta 200 FEG operated in low vacuum mode at 10 kV featured with a backscattered electron detector (BSED). The operational conditions were carefully selected to avoid paraffin melting during the study. The cross-cut of the fibers was done by immersing the samples in liquid nitrogen and stretching them until they broke up with the help of two tweezers. The side cut was made by scalpel at ∼20 °C.

2.4.2. DSC Analysis. DSC was used to determine phase transition temperatures and their corresponding latent heats. DSC was also used to measure the specific heat of fibers, original PVDF powder, and paraffin. A power-compensation DSC Q2500 from TA Instruments was employed with sealed aluminum crucibles. The mass of the samples was ca. 9 mg. Argon (50 mL/min) was employed as the purge gas. Each sample was subjected to three heating and cooling cycles, with a heating/cooling rate of 5 °C/min. The transition temperatures were determined by the onset temperature of the corresponding endothermic peaks in the DSC thermograms, whereas the latent heat was calculated by integrating the latter, assuming a linear baseline. The DSC was calibrated for heat flow and temperature using high purity (>99.99%) reference materials indium and sapphire. The accuracy in determining melting temperatures is ±0.5 °C, whereas the enthalpy of phase transition and specific heat is ±5%.

From the DSC analysis, the PCM content ($PCM_{content}$) can be obtained according to the following equation:

$$PCM_{content}(\%) = \frac{\Delta H_{fiber}}{\Delta H_{paraffin}} \times 100 \quad (1)$$

where ΔH_{fiber} and $\Delta H_{paraffin}$ are the latent heat of composite fibers and paraffin, respectively. On the other hand, eq 2 allows to calculate the encapsulation efficiency (E_e):

$$E_e(\%) = \frac{PCM_{content}}{\left(\frac{paraffin}{PVDF + paraffin}\right)_{feed}} \times 100 \quad (2)$$

where the denominator term represents the theoretical PCM content in the fiber if the encapsulation efficiency was 100%. For the used PVDF:paraffin mass ratio, the denominator term is 50% in all cases.

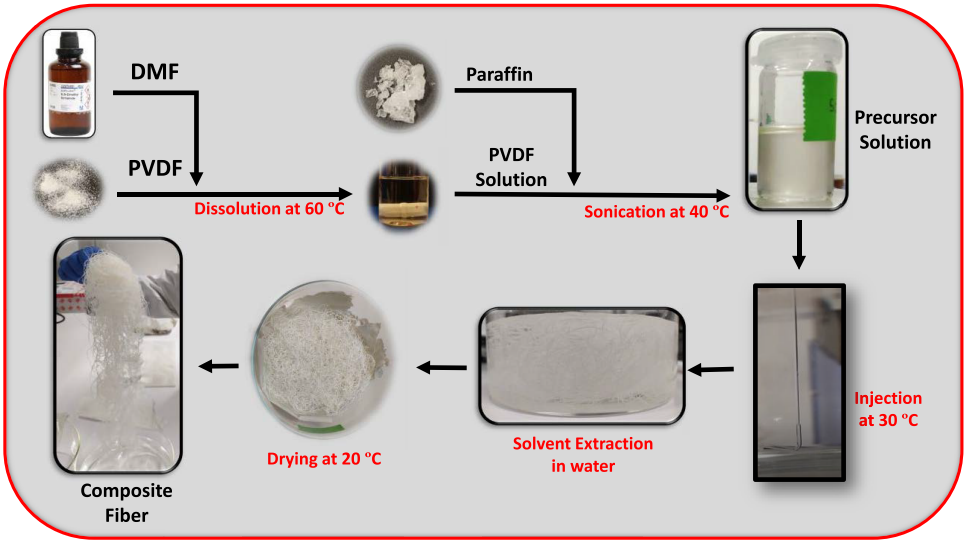

Figure 2. Schematic representation of the production procedure.

https://doi.org/10.1021/acsomega.3c02318
ACS Omega 2023, 8, 26136−26146

The specific heat was determined from the equation of the straight line that fits each thermogram profile. For PVDF-based materials without PCM, the specific heat has been obtained as a function of the temperature in the range of 5−37.5 °C. For PCM-containing fibers, the specific heat has been evaluated in the solid and molten state of PCM. A temperature range from 5 °C to at least 5 °C below the PCM melting temperature was selected for the solid state. For the molten state, a single C_p value was taken at a temperature 5 °C above the T_{offset} (37.5 °C) since the thermogram profile hardly varied with temperature.

2.4.3. Thermal Stability. Thermogravimetric analysis of the fibers and raw materials was performed in a TG209F1 Libra thermogravimetric analyzer from NETZSCH. The analysis was based on a heating ramp from room temperature to 600 °C with a heating rate of 10 °C/min under a nitrogen atmosphere.

2.4.4. Thermal Conductivity. Thermal conductivity of the materials (pelleted PVDF, paraffin, $PVDF_{PCM}$, and $PVDF_{PCM}$ fibers) was characterized by means of the transient plane source (TPS) known as the hot disk method.[31] The latter is based on the use of a flat disk-shaped sensor, a double metal spiral providing both thermal excitation and temperature measurement, sandwiched between two identical samples of the material to be characterized. The size of the sensor and samples, the heating power, and the measurement time were carefully chosen according to the norm Hot Disk ISO 22007-2:2015.[32] Thus, all the samples were first prepared as pellets (cylindrical-shaped, diameter: 13 mm, thickness: ca. 4 mm, see Figure 3) by pressing them in a hydraulic press at 1 ton for 60

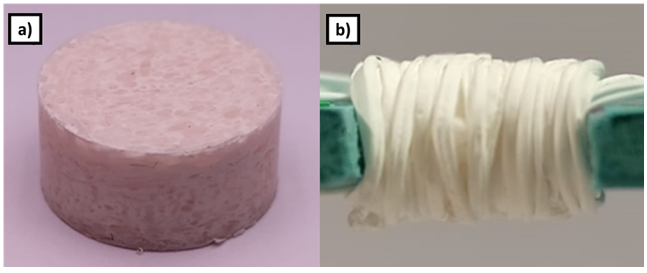

Figure 3. Samples for thermal conductivity measurements. $PVDF_{PCM}$ pellets (a) and rolled fibers (b).

s. A fourth sample was prepared by rolling $PVDF_{PCM}$ fibers onto two supports (see Figure 3). All the measurements were carried out using a Kapton 7577 sensor (radius 2.001 mm) subjected to a heating power from 10 to 20 mW and for a period from 5 to 80 s.

The samples were tested at 20 °C, i.e., below the melting point of the paraffin. The recorded data were processed using the Hot Disk Software (version 7.4.0.10). To assure the reproducibility and the quality of the results, additional tests were carried out on randomly chosen samples, varying operators, heating powers, measurement times, and time ranges for parameter estimation.

2.4.5. Leakage Test. A leakage test was carried out to check the PCM retention capacity of the $PVDF_{PCM}$ fiber. Thus, a piece of $PVDF_{PCM}$ fibers of 200 mg was subjected to 1000 melting/solidification cycles. The fiber was placed onto a Peltier element, covered with absorbing paper, and then pressed with an aluminum block of 61 g (40 × 40 × 13 mm) to ensure a homogeneous temperature distribution and good contact between the fiber and the absorbing paper. Thermal cycles were performed from 10 to 40 °C. Isotherms of 120 s were held at maximum and minimum temperatures for each cycle. Thermal regulation of the Peltier element was ensured using a type K thermocouple and an Arduino Nano coupled with a relay board (Parallax Inc. 27115) and a MAX 31856 module (thermocouple amplifier/converter with integrated cold-junction compensation). The accuracy of the thermocouple module was checked at different temperatures using a temperature-controlled bath (Julabo 1000F) coupled with other systems of temperature measurement (National Instruments NI 9211 and Fluke 233). According to these tests, the accuracy of temperature measurements is less than 2% of a given reading. Software dedicated to thermal regulation and data acquisition was coded with Python 3.7.3, Arduino 1.8.13, and using the Adafruit_MAX31856 library.[33] An extract of the temperature profile of the fiber during the cycles is presented in Figure 4. The fiber mass was checked using a Mettler

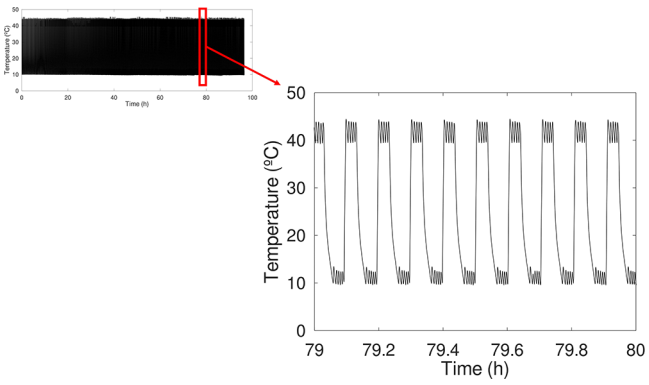

Figure 4. Temperature profile of the $PVDF_{PCM}$ fiber during the leakage test.

Toledo ML304T/00 balance with the accuracy of 0.4 mg at the beginning of the test and after 50, 100, and 1000 cycles to quantify PCM leakage.

2.4.6. Thermal Performance. To study the thermal behavior of the manufactured fibers at a larger scale, four samples of $PVDF_{Hollow}$ and 4 of $PVDF_{PCM}$ fibers were placed in parallel over a Peltier element and subjected to heating/cooling cycles from 10 to 40 °C (see the description of the thermal regulation in Section 2.4.4). The thermal behavior of these samples was recorded during the cycles using an infrared camera (FLIR A6752sc). The camera was configured for data acquisition at 30 Hz in a calibrated temperature range from −20 to 55 °C (integration time was fixed at 3.3 ms). Conversion of the radiometric data to apparent temperatures was performed using the internal calibration curves of the camera and fixing the emissivity of the set of fibers at 0.8.[34] Reflected and atmospheric temperatures were considered constant (20 °C). After cycling, the recorded data were processed using the FLIR software ResearchIR Max Version 4.40.11.35. First, the apparent temperature of each fiber was calculated by averaging the apparent temperatures of a pixel's line drawn along the length of each of them. Then, to visualize more easily the localization of the phase change, a simple image processing based on the subtraction of the tenth image from the current frame (sliding subtraction) was performed.

2.4.7. Mechanical Properties. Tensile stress and strain of the fibers were measured using an Instron 34SC-5 single-column universal testing machine with a 100 N capacity

https://doi.org/10.1021/acsomega.3c02318
ACS Omega 2023, 8, 26136−26146

sensor. Single fibers were placed between the machine clamps with the help of paper "supports/holders". The measurements were carried out at room temperature with a fixed initial gauge length of 20 mm and a stretching rate of 10 mm/min. Measurement accuracy of the column is ±0.5% for load and ±0.02 mm or 0.15% of total displacement (whichever is greater) for strain values. Ten samples of each fiber ($PVDF_{Hollow}$ and $PVDF_{PCM}$) were tested to obtain an average value.

3. RESULTS AND DISCUSSION

3.1. Morphology. SEM images of the surface, cross-section, and axial section of both $PVDF_{Hollow}$ and $PVDF_{PCM}$ fibers are presented in Figure 5. First, one can see that the

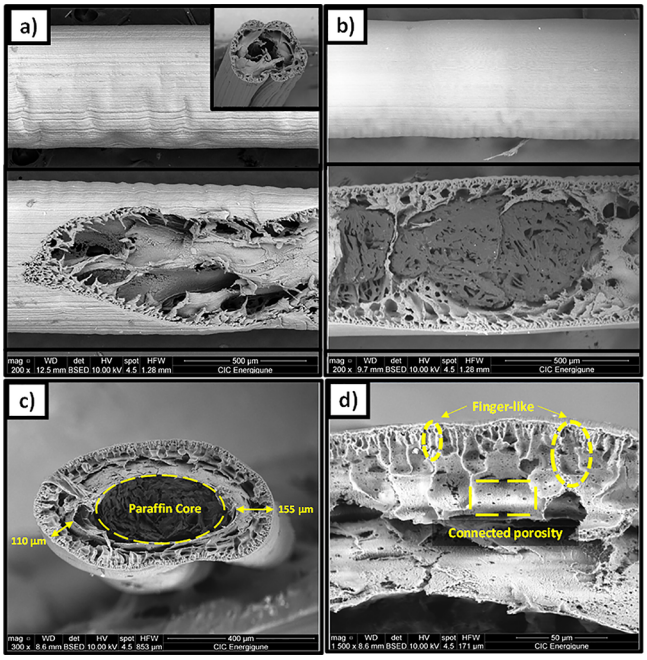

Figure 5. SEM images of $PVDF_{Hollow}$ and $PVDF_{PCM}$ fibers: (a) side and cross-cut views of $PVDF_{Hollow}$ fibers; (b) side views of $PVDF_{PCM}$ fibers; (c and d) cross-cut views of $PVDF_{PCM}$ fibers.

outer diameter of the produced fibers is very close to the internal diameter of the glass capillary used for injection, which is around 0.5 mm. The wall thickness of the fibers is between 100 and 200 μm (Figure 5c). The exterior surface of both fibers consists of a dense PVDF without imperfections or holes (Figure 5a,b). Even so, it has to be mentioned that polymeric fibers produced by solvent extraction tend to present nanopores on their surface due to solvent diffusion.[35,36]

According to the images, $PVDF_{Hollow}$ fibers are covered by longitudinal folds, while the surface of the $PVDF_{PCM}$ fibers is flatter (see Figure 5a, b). Those folds are a consequence of the solvent extraction and drying processes. In the case of $PVDF_{PCM}$ fibers, the paraffin plays the role of support and decreases the solvent extraction rate, resulting in a smoother surface. The effective density of the PVDF fibers produced by solvent extraction varies versus their diameter. It has its maximum at the fiber's wall and decreases until zero or near zero value at the central axis. The finger-like pore can be observed close to the outer wall (see Figure 5d), which is typical of nonsolvent-induced solvent extraction (NIPS) processes.[20,28,29] In the presented system, DMF acts as a solvent and water as a nonsolvent for the polymer (PVDF). When the precursor jet comes out from the glass capillary, a NIPS process starts due to the miscibility between water and DMF. At this moment, the high rate of DMF extraction promotes PVDF concentration increase and a decrease of solvent concentration. Finally, the polymer solidifies and forms an outer dense wall of the final fibers. As the NIPS process goes on, the internal phase of the precursor jet starts to separate in polymer-rich and polymer-lean phases, promoting the formation of the porous structure.[37] The pore size increases as the solvent amount in the precursor jet decreases. Consequently, fibers exhibit a hierarchical structure, where the largest macro pore "channel" on the order of 200−300 μm is located in the middle of the fiber, whereas the fiber's walls have two characteristic size ranges of pores, 4−50 μm and less than 2 μm.

The $PVDF_{PCM}$ fibers have a core-shell structure where the mentioned PVDF hierarchical porous structure wraps the paraffin (core). This hierarchical structure allows withstanding volume changes during the melting of the paraffin.[3] Furthermore, the outer wall is smooth, dense, and homogeneous, which indicates that it forms a sealed container that will help to avoid PCM leakage. Figure 5b shows that the paraffin is distributed in a form of slugs along the fiber. These slugs differ in size and are separated by PVDF walls along all the fiber length.

3.2. Thermal Properties. *3.2.1. DSC Analysis.* The melting point and corresponding latent heat of paraffin (RT-28HC) and the synthesized $PVDF_{PCM}$ fibers were measured by DSC. Figure 6 shows the obtained thermograms for pure PCM

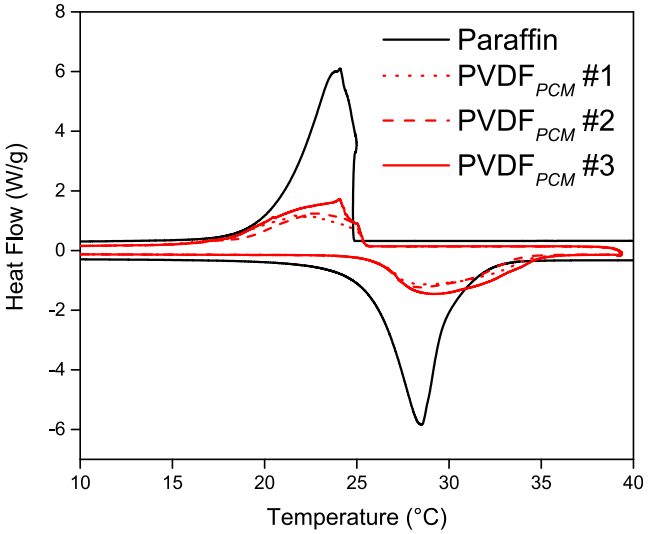

Figure 6. DSC thermograms of pure paraffin and different samples from the obtained $PVDF_{PCM}$ fibers.

and the $PVDF_{PCM}$ fiber samples. The fiber samples were randomly selected from the same fiber. Onset temperatures ($Tonset_m$, $Tonset_c$), latent heat values (ΔH_m, ΔH_c), PCM contents, and calculated encapsulation efficiencies are given in Table 1.

As shown in Figure 6, both paraffin and the $PVDF_{PCM}$ fibers present a single endothermic peak during the heating and cooling. Melting starts at 25.7 °C for paraffin and 26.2 °C for all the $PVDF_{PCM}$ fiber samples. The paraffin's melting and crystallization onset temperatures move to slightly higher

https://doi.org/10.1021/acsomega.3c02318
ACS Omega 2023, 8, 26136−26146

Table 1. Transition Temperatures, Latent Heat, PCM Content, and Encapsulation Efficiency Values of the Paraffin and $PVDF_{PCM}$ Fibers

sample	$Tonset_m$ (°C)	ΔH_m (J/g)	$Tonset_c$ (°C)	ΔH_c (J/g)	$PCM_{content}$ (%)	E_e (%)
RT-28HC	25.7	247	24.7	247		
$PVDF_{PCM}$ #1	26.2	75	25.3	75	30	61
$PVDF_{PCM}$ #2	26.2	73	25.3	72	29	59
$PVDF_{PCM}$ #3	26.2	98	25.4	97	39	79

Table 2. C_p Values for the Produced Fibers and Their Pure Components

	solid state	liquid state $_{(37.5°C)}$
sample	equation (J/g °C)	value (J/g °C)
$PVDF_{Powder}$	$0.995 + 0.004 \times T_{(5-37.5°C)}$	
$PVDF_{Hollow}$ #1	$1.056 + 0.004 \times T_{(5-37.5°C)}$	
$PVDF_{Hollow}$ #2	$1.171 + 0.004 \times T_{(5-37.5°C)}$	
$PVDF_{Hollow}$ #3	$1.165 + 0.004 \times T_{(5-37.5°C)}$	
Paraffin	$1.486 + 0.024 \times T_{(5-15°C)}$	2.156
$PVDF_{PCM}$ #1	$1.277 + 0.020 \times T_{(5-20°C)}$	1.576
$PVDF_{PCM}$ #2	$1.262 + 0.020 \times T_{(5-20°C)}$	1.530
$PVDF_{PCM}$ #3	$1.322 + 0.019 \times T_{(5-20°C)}$	1.603

temperatures when the PCM is encapsulated into the fibers. This may indicate that adding the polymeric fiber shell to the paraffin enhances its recrystallization and increases its melting point.[20]

All tested samples have shown latent heat values of melting between 73 and 98 J/g, with a coefficient of variation of 13%. Compared to the latent heat of pure paraffin (247 J/g) and using eq 1, the PCM content lies between 29 and 39%. This variation of the PCM content of randomly chosen samples is related to the nonhomogeneous distribution of the paraffin along the $PVDF_{PCM}$ fibers. Although the emulsion was stable during $PVDF_{PCM}$ fiber production, at the solvent extraction stage, a strong gradient of PVDF and DMF forces the coalescence of paraffin droplets in larger paraffin fractions, which leads to the observed slugs. A possible strategy to increase the PCM content of the fibers could be the addition of more PCM to the fiber precursors. Nevertheless, this approach has limitations as too high PCM contents in the precursors drastically affect the stability of the PCM emulsions, giving place to the rupture of the precursor jet during injection and loss of PCM.

Finally, the encapsulation efficiency is in the range of 60−80%, which is a good result for a "proof of concept" of a new production method. Two main factors should be considered to understand the values of encapsulation efficiency. First, the jet formation is by a precursor emulsion. It can be assumed that a certain amount of PCM droplets will be located in the edges of the jet, being able to escape before being encapsulated. Second, the strong solvent extraction at the beginning of the NIPS process can displace some paraffin outside the jet before the outer layer of the fibers solidifies, reducing the PCM content and the encapsulation efficiency. Hence, the fiber production method could be further improved by controlling the PCM droplet position inside the precursor jet, applying, for example, swirling flows injection or using coaxial flows for emulsion formation by microfluidics devices. The increase of the encapsulation efficiency is also possible by controlling the solvent extraction rate through the optimization of parameters such as injection flow rates, solid content in the precursor solutions, solvent extraction bath temperature, or applying other liquid for solvent extraction instead of water.

Table 2 indicates the specific heat capacity obtained from DSC analysis of the fibers and the constituent elements (PVDF powder and paraffin). $PVDF_{Hollow}$ fibers present higher C_p values than that for pure PVDF powder, while the temperature dependence of C_p is the same. The higher C_p values of $PVDF_{Hollow}$ fibers reveal their lower degree of crystallinity than the supplied PVDF powder.[38] Moreover, the C_p of the $PVDF_{PCM}$ fiber is even higher, reaching values between 1.53 and 1.60 J/g K at 37.5 °C due to the presence of paraffin, which has a higher C_p.

3.2.2. Thermal Stability (TGA). TGA and DTG profiles of pure paraffin, PVDF powder, $PVDF_{Hollow}$ fiber, and $PVDF_{PCM}$ fiber are presented in Figure 7. As can be seen, paraffin RT-28HC is thermally stable until 179.8 °C. Thermal degradation (evaporation) starts and reaches its maximum rate at 224.5 °C with no residue at the end of the process. Pure PVDF powder presents good thermal stability up to 360 °C. Then, it follows two degradation peaks: the lower one at 411 °C and the maximum one at 478.2 °C.

Similar to the pure PVDF powder, two main degradation peaks can be observed for the three samples of $PVDF_{Hollow}$ fibers. The onset of the degradation takes place at 300 °C, which is 53.3 °C lower than that for PVDF powder. The first minor peak appears at 349 °C and the second major one at 469.6 °C. As one can see, the onset and both degradation peaks are shifted to the lower temperatures for the three samples of $PVDF_{Hollow}$ fibers compared to PVDF powder. This indicates the change in crystallinity of the PVDF due to the rapid crystallization by the solvent extraction method.[39]

Finally, the $PVDF_{PCM}$ fibers present three main degradation peaks. The first one appears at an average temperature of 230.8 °C and is related to the fibers' paraffin content, which varies from 31.8 to 47.5%. This variation is a consequence of the already mentioned nonhomogeneous distribution of the paraffin inside the fibers, which could be seen in SEM images and that also affected the encapsulation efficiency variations of the DSC analysis results.

It must be mentioned that the average decomposition temperature of the encapsulated paraffin is 6 °C higher than that obtained for the pure PCM, which indicates that the PVDF sheath of the fibers is protecting the PCM from thermal degradation (evaporation). The onset of the PVDF degradation appears at 300 °C, similar to that of $PVDF_{Hollow}$ fibers. However, the second peak occurs at 353.3 °C and the third at 473.3 °C. Both peaks corresponding to PVDF degradation are at ∼4 °C higher than that for $PVDF_{Hollow}$ fibers. This is in coherence with the results on the specific heat of produced fibers and confirms higher crystallinity of PVDF in $PVDF_{PCM}$ fibers.

3.2.3. Thermal Conductivity (Hot Disk). The values of thermal conductivity obtained by the Hot Disk method are presented in Table 3. The PVDF and paraffin pellets have thermal conductivities of 0.189 and 0.571 W/m K, respectively, while the pelletized $PVDF_{PCM}$ fiber has a thermal conductivity of 0.287 W/m K. The obtained results were then cross-validated by applying different models of effective thermal conductivity of a two-phase mixture. The conventional

https://doi.org/10.1021/acsomega.3c02318
ACS Omega 2023, 8, 26136−26146

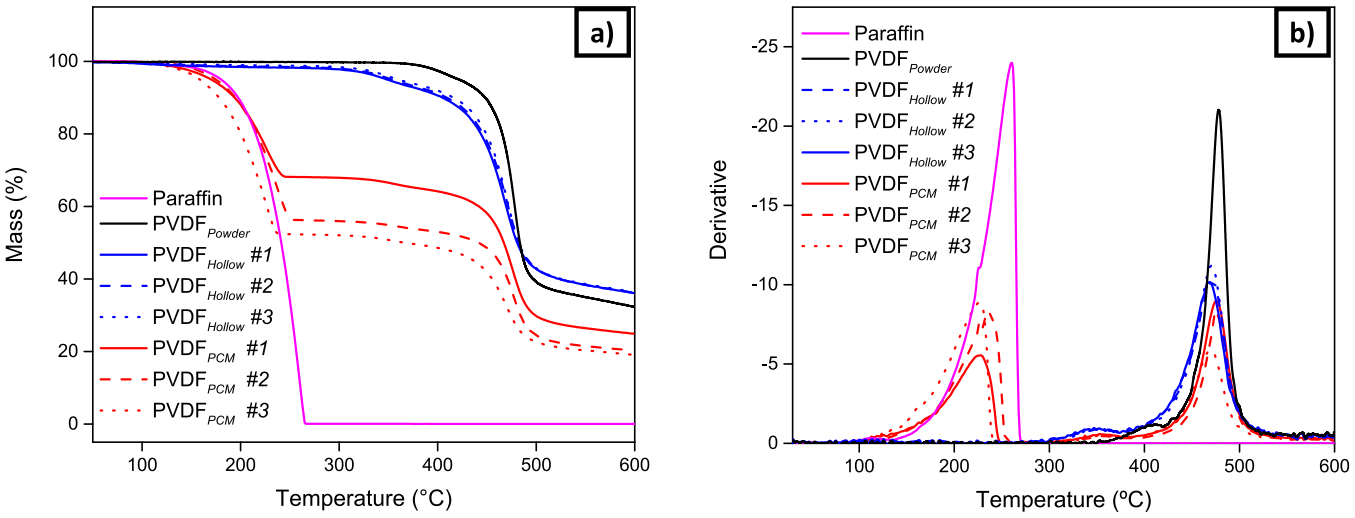

Figure 7. TGA (a) and DTG (b) profiles of pure paraffin, PVDF powder, $PVDF_{Hollow}$ fibers, and $PVDF_{PCM}$ fibers.

Table 3. Thermal Conductivity of Pure PVDF, Paraffin and the Produced $PVDF_{PCM}$ Fibers

sample	therm. cond. (W/m K)	ave. dev. (W/m K)	ave. dev. (%)
PVDF (pellet)	0.189	0.001	0.8
paraffin (pellet)	0.571	0.022	3.8
$PVDF_{PCM}$ fiber (pellet)	0.287	0.030	10.3
$PVDF_{PCM}$ fiber (rolled)	0.063	0.002	2.7

series and parallel mixture rule[40] leads to a thermal conductivity ranging between 0.24 and 0.31 W/m K for the pelletized $PVDF_{PCM}$ fibers. The most restrictive model[41,42] allows the determination of 0.27 W/m K for the lower bound and 0.29 W/m K for the upper bound, which is in very good agreement with the experimentally measured thermal conductivity of 0.287 W/m K.

The transverse thermal conductivity of rolled $PVDF_{PCM}$ fibers was also measured by the Hot Disk method. In this case, the measured value was 0.063 W/m K which is much lower compared to the pure components. This result for "as-synthesized" fibers was expected due to their high porosity. Moreover, the interfiber porosity of the rolled $PVDF_{PCM}$ fibers also affects the resulting effective thermal conductivity.

The low thermal conductivity and high elasticity of produced fibers (to be discussed in Section 3.5) suggest that they can be applied as thermal insulation materials with thermal buffer properties. Such materials are of great interest for building applications,[43] smart textiles,[44] and electric battery thermal management in cold climate.[45] Nevertheless, simple pelletizing of the $PVDF_{PCM}$ fibers allows to recover thermal conductivity to the values of nonporous PVDF/PCM composites that can be applied in thermal energy storage applications. Moreover, applying different forces between 0 and 1 Tonn, thermal conductivity can be potentially tuned in a quiet wide range 0.063−0.287 W/(m K).

3.3. PCM Retention Capacity. The produced $PVDF_{PCM}$ fiber was submitted to 1000 heating/cooling cycles from 10 to 40 °C with 120 s of isothermal periods at both temperatures. In total, the sample was subjected to thermal cycling for almost 100 h. The DSC thermogram of the fiber after thermal cycling is presented in Figure 8. The weight loss of the sample was

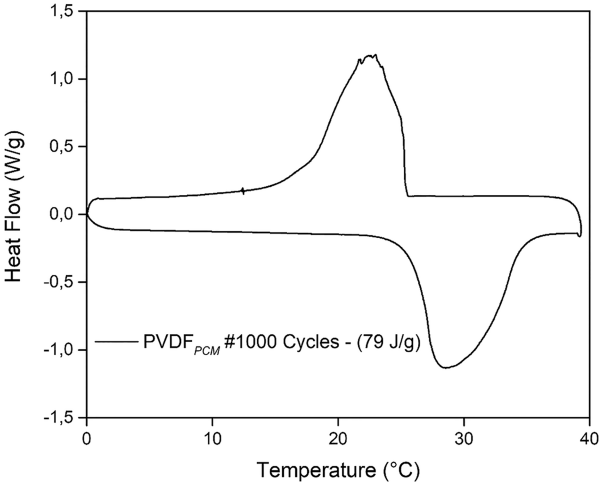

Figure 8. DSC thermogram of the $PVDF_{PCM}$ fiber after 1000 heating−cooling cycles.

0.84 wt % after the first 50 cycles, 1.06 wt % after the 100th cycle, and stays below 3.5 wt % after 1000 cycles. The DSC analysis after thermal cycling shows that the sample preserves its melting transition, which starts at 26.2 °C and that has an associated latent heat of melting of 79 J/g. This new enthalpy value falls within the standard deviation range observed for the noncycled fibers. Even though no precautions were undertaken to close the ends of the fibers, the results indicate that the composite fiber efficiently retains the molten PCM inside its structure, prevents leakage, and maintains thermal storage capacity. This cycling stability corresponds to a cycling category C according to the Quality and Testing Specifications for Phase Change Materials − PCM, by the German Institute for Quality Assurance and Certification Association.[46] Such good results can be explained by "two stage" leakage protection. The first stage is a porous structure that acts as a shape-stabilizing material. Our previous work demonstrated that hierarchical porosity enhances the anti-leakage performance of shape-stabilized PCMs.[3] It was shown that secondary smaller porosity located at the walls of the large central pore significantly enhances capillary forces in the main large pore and contributes to better leak prevention. The second stage of protection is an outer dens wall of the fiber that acts as a

https://doi.org/10.1021/acsomega.3c02318
ACS Omega 2023, 8, 26136−26146

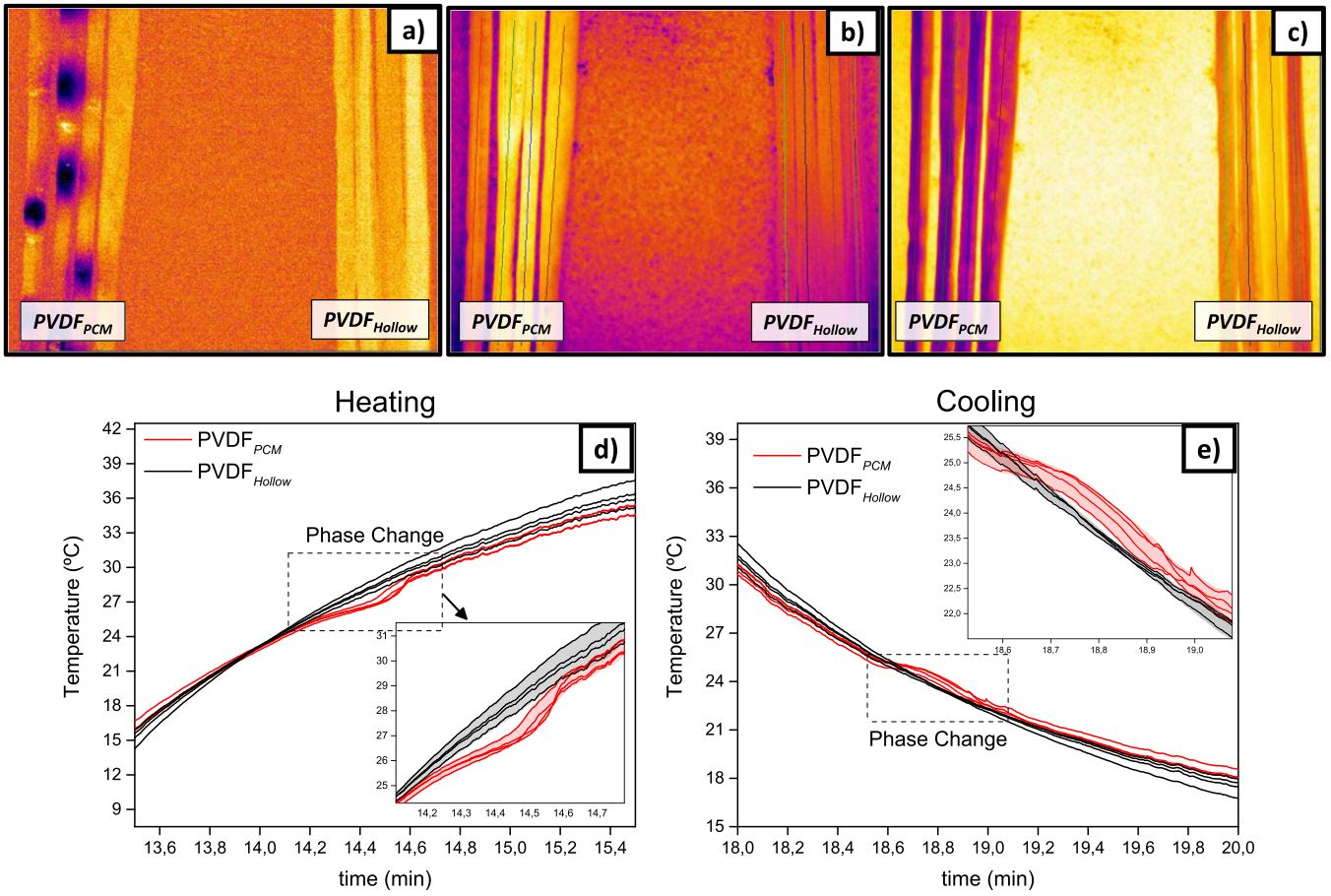

Figure 9. Thermal images of the fibers during the first cycle heating (a), first cycle cooling (b), and second cycle heating (c). Thermal profiles of the fibers during heating (d) and cooling (e).

"classical" sheath. Thus, PCM-containing fibers produced here benefit from both approaches to deal with leaks, i.e., shape stabilization and encapsulation. Moreover, the morphology of the fibers described above suggests that the large inside channel should help spreading the molten paraffin in the longitudinal direction and better penetration to the smaller pores. The spreading of the paraffin along the fiber in dynamics was studied with the help of the infrared camera and will be discussed below.

3.4. Infrared Analysis of Thermal Performance. The temperature evolution of the fibers when they are subjected to thermal cycles between 10 and 40 °C was followed by an infrared camera (Figure 9a, b, c), and the results obtained during one heating and cooling cycles are presented in Figure 9d,e, where the average apparent temperature along the length of each fiber is shown. One can notice that despite uncertainty on the real emissivity of the fibers, the melting and crystallization temperatures agree with those obtained by standard DSC measurements, being the T_{onset} both in charging and discharging between 25 and 26 °C. It is evident from the graph that the slope of the temperature profiles decreases when the temperature reaches the PCM melting point, which indicates that the heat is being used for the melting process instead of the temperature increase. Therefore, the fibers gain thermal buffer properties by incorporating PCM.

A second data processing was carried out based on a sliding subtraction of the recorded images to facilitate tracking the location of the phase change along each fiber. Thanks to the large observation scale offered by the IR camera, it can be seen that, during the first cycle, the phase change is highly localized in space (see Figure 9a, and Video S1 provided in the Supporting Information, where $PVDF_{PCM}$ fibers appear on the left side and $PVDF_{Hollow}$ fibers appear on the right side), which implies a heterogeneous distribution of the PCM in slugs, as previously described. However, in subsequent thermal cycling, the PCM is no longer observed localized but becomes homogeneously distributed from the second cycle onward due to the spread of the PCM through the fiber (see Figure 9c, and Video S2 provided in the Supporting Information, where $PVDF_{PCM}$ fibers appear on the left side and $PVDF_{Hollow}$ fibers appear on the right side). This flow of PCM inside the fibers is driven by capillary forces when it is in the liquid phase.

3.5. Mechanical Properties. The tensile stress of fibers can be obtained by considering the ratio of force corresponding to the cross-sectional area of the fibers (Pa) or the ratio of load to the linear density of the fibers (N/tex). For the case of the fibers produced in this work, which are hollow and porous, it is not easy to precisely measure their cross-sectional dimensions, so the N/tex units have been selected. Therefore, errors in the results due to high sensitivity to the diameter measurements of the fibers are avoided.[47] Each fiber sample was weighed and measured to obtain the linear density of every gauge, and 10 different samples of each fiber were tested.

The effect of paraffin addition on the mechanical properties of the PVDF fibers is presented in Figure 10, where the mean

https://doi.org/10.1021/acsomega.3c02318
ACS Omega 2023, 8, 26136−26146

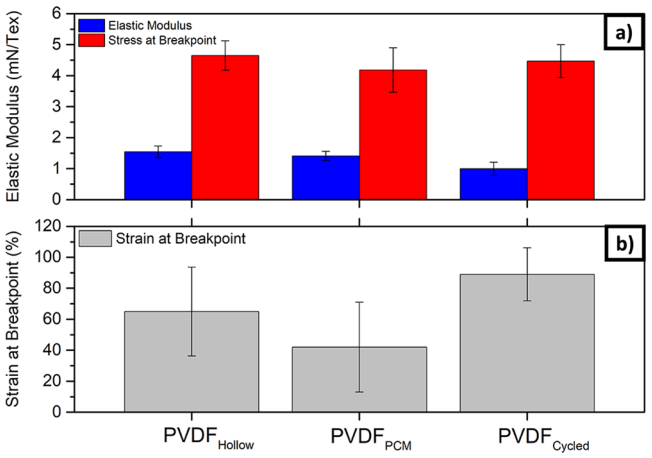

Figure 10. Mechanical properties of the fibers; (a): Elastic modulus and stress at breakpoint and (b): Strain at the breakpoint.

values of elastic modulus, stress at breakpoint, and strain at breakpoint of $PVDF_{Hollow}$ and $PVDF_{PCM}$ fibers are shown, as well as the values obtained for a fiber that was previously submitted to 1000 thermal cycles ($PVDF_{Cycled}$).

Results show that the tested fibers present similar elastic modulus and stress at the breakpoint with values in the range of 1−1.5 and 4−5 mN/Tex, respectively (Figure 10a), which are comparable to the ones obtained by other authors.[29] Therefore, the addition of PCM to the PVDF fibers and the thermal cycling is not affecting the fiber's mechanical resistance. Nevertheless, different behaviors can be appreciated for the maximum elongation of the fibers (Figure 10b). $PVDF_{Hollow}$ and $PVDF_{PCM}$ fibers present elongation values between 40 and 65% at the breakpoint, while the mean value for the $PVDF_{Cycled}$ fibers increases up to 89%. As seen in the SEM images, PCM was distributed in a form of slugs all along the fibers' axial direction. These separate PCM slugs were later redistributed and homogenized in the fibers' inner porous structure during the first melting cycle (confirmed by IR thermography), considerably improving the elasticity of the $PVDF_{PCM}$ fibers and their strain at the breakpoint.

4. CONCLUSIONS

The present work presents a versatile method for the in situ fabrication of thermoregulating PVDF fibers containing PCM. The method is based on the microfluidics approach, emulsion injection, and solvent extraction to produce both hollow fibers and composite PVDF-based fibers with PCM contents between 30 and 47.5 wt %. The proposed approach results in fibers with up to 98 J/g of latent heat, with a hierarchical porous structure where the paraffin is distributed in a form of slugs along the fiber. However, although the PCM is initially located in the form of slugs along the fiber, thermal cycling distributes the PCM homogeneously along the fiber. The high porosity of composite fibers suppresses thermal conductivity down to 0.063 W/m K. However, simple pelletizing of the $PVDF_{PCM}$ fibers makes it possible to recover thermal conductivity to the value of nonporous $PVDF_{PCM}$ composite that is 0.287 W/m K. Furthermore, the produced $PVDF_{PCM}$ fibers revealed an outstanding retention capacity of molten PCM after 1000 thermal cycles. Finally, it has been shown that the presence of PCM does not considerably affect the mechanical properties of the obtained fibers. The results here reaffirm the potential that the PVDF-PCM combo presents for applications requiring simultaneously thermal management and low thermal conductivity, demonstrating the benefits of its thermophysical properties and a manufacturing process simplicity that can be easily scaled up.

ASSOCIATED CONTENT

Supporting Information

The Supporting Information is available free of charge at https://pubs.acs.org/doi/10.1021/acsomega.3c02318.

Scheme of the experimental setup for fiber production; schematic representation of the production procedure; temperature profiles; SEM images; DSC thermograms; GA and DTG profiles; thermal images; and mechanical properties (PDF)

Video 1 (AVI)

Video 2 (AVI)

AUTHOR INFORMATION

Corresponding Author

Artem Nikulin − *Centre for Cooperative Research on Alternative Energies (CIC energiGUNE), Basque Research and Technology Alliance (BRTA), 01510 Vitoria-Gasteiz, Spain;* orcid.org/0000-0002-3304-0506; Email: anikulin@cicenergigune.com

Authors

Mikel Duran − *Centre for Cooperative Research on Alternative Energies (CIC energiGUNE), Basque Research and Technology Alliance (BRTA), 01510 Vitoria-Gasteiz, Spain; University of the Basque Country (UPV/EHU), 20018 Donostia-San Sebastián, Gipuzkoa, Spain*

Angel Serrano − *Centre for Cooperative Research on Alternative Energies (CIC energiGUNE), Basque Research and Technology Alliance (BRTA), 01510 Vitoria-Gasteiz, Spain*

Jean-Luc Dauvergne − *Centre for Cooperative Research on Alternative Energies (CIC energiGUNE), Basque Research and Technology Alliance (BRTA), 01510 Vitoria-Gasteiz, Spain*

Yaroslav Grosu − *Centre for Cooperative Research on Alternative Energies (CIC energiGUNE), Basque Research and Technology Alliance (BRTA), 01510 Vitoria-Gasteiz, Spain; Institute of Chemistry, University of Silesia in Katowice, 40-006 Katowice, Poland;* orcid.org/0000-0001-6523-1780

Jalel Labidi − *University of the Basque Country (UPV/EHU), 20018 Donostia-San Sebastián, Gipuzkoa, Spain*

Elena Palomo del Barrio − *Centre for Cooperative Research on Alternative Energies (CIC energiGUNE), Basque Research and Technology Alliance (BRTA), 01510 Vitoria-Gasteiz, Spain; Ikerbasque, Basque Foundation for Science, 48013 Bilbao, Spain*

Complete contact information is available at: https://pubs.acs.org/10.1021/acsomega.3c02318

Author Contributions

M.D.: Writing original draft, Formal analysis, Investigation, Visualization, Writing-review & editing. A.N.: Conceptualization, Writing original draft, Methodology, Formal analysis, Supervision, Investigation, Visualization, Writing-review & editing. J.-L.D.: Methodology, Formal analysis, Investigation, Visualization, Writing-review & editing. A.S.: Supervision,

https://doi.org/10.1021/acsomega.3c02318
ACS Omega 2023, 8, 26136−26146

Formal analysis, Writing-review & editing. Y.G.: Formal analysis, Writing-review & editing. J.L.: Supervision, Writing-review & editing. E.P.D.B.: Supervision, Writing-review & editing, Funds acquisition.

Notes

The authors declare no competing financial interest.

■ ACKNOWLEDGMENTS

The authors are grateful for the financial support from SWEET-TES project (RTI2018-099557-B-C21), funded by FEDER/Ministerio de Ciencia e Innovación - Agencia Estatal de Investigación and Elkartek CICe2020 project (KK-2020/00078) funded by Basque Government. Mikel Duran Lopez would also like to thank the Department of Education, Linguistic Politics and Culture of the Basque Country government for the granted pre-doctoral contract (PRE_2019_1_0154). This article is part of the grant RYC2021-032445-I funded by MICIN/AEI/10.13039/501100011033 and by the European Union NextGenerationEU/PRTR.

■ REFERENCES

(1) Chidambaranathan, B.; Vijayaram, M.; Suriya, V.; Sai Ganesh, R.; Soundarraj, S. A Review on Thermal Issues in Li-Ion Battery and Recent Advancements in Battery Thermal Management System. *Mater. Today Proc.* **2020**, *33*, 116−128.

(2) Kumar, P.; Chaudhary, D.; Varshney, P.; Varshney, U.; Yahya, S. M.; Rafat, Y. Critical Review on Battery Thermal Management and Role of Nanomaterial in Heat Transfer Enhancement for Electrical Vehicle Application. *J. Energy Storage* **2020**, *32*, No. 102003.

(3) Grosu, Y.; Zhao, Y.; Giacomello, A.; Meloni, S.; Dauvergne, J. L.; Nikulin, A.; Palomo, E.; Ding, Y.; Faik, A. Hierarchical Macro-Nanoporous Metals for Leakage-Free High-Thermal Conductivity Shape-Stabilized Phase Change Materials. *Appl. Energy* **2020**, *269*, No. 115088.

(4) Wei, H.; Yang, S.; Wang, C.; Qiu, C.; Lin, K.; Han, J.; Lu, Y.; Liu, X. Novel and Durable Composite Phase Change Thermal Energy Storage Materials with Controllable Melting Temperature. *J. Mater. Sci. Technol.* **2021**, *86*, 11−19.

(5) Chen, F.; Huang, R.; Wang, C.; Yu, X.; Liu, H.; Wu, Q.; Qian, K.; Bhagat, R. Air and PCM Cooling for Battery Thermal Management Considering Battery Cycle Life. *Appl. Therm. Eng.* **2020**, *173*, No. 115154.

(6) Szczotok, A. M.; Madsen, D.; Serrano, A.; Carmona, M.; Van Hees, P.; Rodriguez, J. F.; Kjøniksen, A. L. Flame Retardancy of Rigid Polyurethane Foams Containing Thermoregulating Microcapsules with Phosphazene-Based Monomers. *J. Mater. Sci.* **2021**, *56*, 1172−1188.

(7) Borreguero, A. M.; Valverde, J. L.; Rodríguez, J. F.; Barber, A. H.; Cubillo, J. J.; Carmona, M. Synthesis and Characterization of Microcapsules Containing Rubitherm RT27 Obtained by Spray Drying. *Chem. Eng. J.* **2011**, *166*, 384.

(8) Cárdenas-Ramírez, C.; Jaramillo, F.; Gómez, M. Systematic Review of Encapsulation and Shape-Stabilization of Phase Change Materials. *J. Energy Storage* **2020**, *30*, No. 101495.

(9) Ola, O.; Chen, Y.; Niu, Q.; Xia, Y.; Mallick, T.; Zhu, Y. Ultralight Three-Dimensional, Carbon-Based Nanocomposites for Thermal Energy Storage. *J. Mater. Sci. Technol.* **2020**, *36*, 70−78.

(10) Shin, Y.; Il Yoo, D.; Son, K. Development of Thermoregulating Textile Materials with Microencapsulated Phase Change Materials (PCM). II. Preparation and Application of PCM Microcapsules. *J. Appl. Polym. Sci.* **2005**, *96*, 2005−2010.

(11) Yan, Y.; Li, W.; Zhu, R.; Lin, C.; Hufenus, R. Flexible Phase Change Material Fiber: A Simple Route to Thermal Energy Control Textiles. *Materials* **2021**, *14*, 401.

(12) Chen, C.; Wang, L.; Huang, Y. A Novel Shape-Stabilized PCM: Electrospun Ultrafine Fibers Based on Lauric Acid/Polyethylene Terephthalate Composite. *Mater. Lett.* **2008**, *62*, 3515−3517.

(13) Nguyen, T. T. T.; Lee, J. G.; Park, J. S. Fabrication and Characterization of Coaxial Electrospun Polyethylene Glycol/Polyvinylidene Fluoride (Core/Sheath) Composite Non-Woven Mats. *Macromol. Res.* **2011**, *19*, 370−378.

(14) Xia, W.; Fei, X.; Wang, Q.; Lu, Y.; Innocent, M. T.; Zhou, J.; Yu, S.; Xiang, H.; Zhu, M. Nano-Hybridized Form-Stable Ester@F-SiO2 Phase Change Materials for Melt-Spun PA6 Fibers Engineered towards Smart Thermal Management Fabrics. *Chem. Eng. J.* **2021**, *403*, No. 126369.

(15) Deng, Y.; Li, J.; Qian, T.; Guan, W.; Wang, X. Preparation and Characterization of KNO3/Diatomite Shape-Stabilized Composite Phase Change Material for High Temperature Thermal Energy Storage. *J. Mater. Sci. Technol.* **2017**, *33*, 198−203.

(16) Hu, W.; Yu, X. Encapsulation of Bio-Based PCM with Coaxial Electrospun Ultrafine Fibers. *RSC Adv.* **2012**, *2*, 5580−5584.

(17) Golestaneh, S. I.; Mosallanejad, A.; Karimi, G.; Khorram, M.; Khashi, M. Fabrication and Characterization of Phase Change Material Composite Fibers with Wide Phase-Transition Temperature Range by Co-Electrospinning Method. *Appl. Energy* **2016**, *182*, 409−417.

(18) Babapoor, A.; Karimi, G.; Golestaneh, S. I.; Mezjin, M. A. Coaxial Electro-Spun PEG/PA6 Composite Fibers: Fabrication and Characterization. *Appl. Therm. Eng.* **2017**, *118*, 398−407.

(19) Darzi, M. E.; Golestaneh, S. I.; Kamali, M.; Karimi, G. Thermal and Electrical Performance Analysis of Co-Electrospun-Electrosprayed PCM Nanofiber Composites in the Presence of Graphene and Carbon Fiber Powder. *Renewable Energy* **2019**, *135*, 719−728.

(20) Xiang, L.; Luo, D.; Yang, J.; Sun, X.; Jin, J.; Qin, S. Construction and Design of Paraffin/PVDF Hollow Fiber Linear-Phase Change Energy Storage Materials. *Energy Fuels* **2019**, *33*, 11584−11591.

(21) Sun, Z.; Zussman, E.; Yarin, A. L.; Wendorff, J. H.; Greiner, A. Compound Core−Shell Polymer Nanofibers by Co-Electrospinning. *Adv. Mater.* **2003**, *15*, 1929−1932.

(22) Reneker, D. H.; Yarin, A. L. Electrospinning Jets and Polymer Nanofibers. *Polymer* **2008**, *49*, 2387−2425.

(23) Zdraveva, E.; Fang, J.; Mijovic, B.; Lin, T. Electrospun Poly(Vinyl Alcohol)/Phase Change Material Fibers: Morphology, Heat Properties, and Stability. *Ind. Eng. Chem. Res.* **2015**, *54*, 8706−8712.

(24) PVDF binder for batteries, 2022. https://nanografi.com/blog/pvdf-binder-for-battery/.

(25) Comercial PVDF, 2022. https://www.swicofil.com/commerce/products/pvdf/299/introduction.

(26) Song, Y. N.; Lei, M. Q.; Lei, J.; Li, Z. M. Spectrally Selective Polyvinylidene Fluoride Textile for Passive Human Body Cooling. *Mater. Today Energy* **2020**, *18*, No. 100504.

(27) Haghighat, F.; Hosseini Ravandi, S. A.; Nasr Esfahany, M.; Valipouri, A. A Comprehensive Study on Optimizing and Thermo-regulating Properties of Core−Shell Fibrous Structures through Coaxial Electrospinning. *J. Mater. Sci.* **2018**, *53*, 4665−4682.

(28) Wen, G. Q.; Xie, R.; Liang, W. G.; He, X. H.; Wang, W.; Ju, X. J.; Chu, L. Y. Microfluidic Fabrication and Thermal Characteristics of Core−Shell Phase Change Microfibers with High Paraffin Content. *Appl. Therm. Eng.* **2015**, *87*, 471−480.

(29) Zhang, X.; Xie, R.; Hu, W. X.; Faraj, Y.; Zhao, Q.; Fan, X. X.; Wang, W.; Ju, X. J.; Liu, Z.; Chu, L. Y. Microfluidic Fabrication of Core−Sheath Composite Phase Change Microfibers with Enhanced Thermal Conductive Property. *J. Mater. Sci.* **2018**, *53*, 15769−15783.

(30) Rubitherm rt28hc data sheet, 2020. https://www.rubitherm.eu/media/products/datasheets/Techdata_-RT28HC_EN_09102020.PDF.

(31) Gustafsson, S. E. Transient Plane Source Techniques for Thermal Conductivity and Thermal Diffusivity Measurements of Solid Materials. *Rev. Sci. Instrum.* **1991**, *62*, 797−804.

https://doi.org/10.1021/acsomega.3c02318
ACS Omega 2023, 8, 26136−26146

(32) DIN EN ISO 22007-2:2021-05. Plastics - Determination of Thermal Conductivity and Thermal Diffusivity - Part 2: Transient Plane Heat Source (Hot Disc) Method (ISO/DIS 22007-2:2021).
(33) Arduino library for adafruit max31856, 2021. https://github.com/adafruit/Adafruit_MAX31856.
(34) Fujikura, Y.; Suzuki, T.; Matumoto, M. Measurements of Thermal Emissivity of Polymers. *Sen'i Gakkaishi* **1975**, *31*, T445−T447.
(35) Na, H.; Chen, P.; Wong, S. C.; Hague, S.; Li, Q. Fabrication of PVDF/PVA Microtubules by Coaxial Electrospinning. *Polymer* **2012**, *53*, 2736−2743.
(36) Ji, G. L.; Zhu, L. P.; Zhu, B. K.; Zhang, C. F.; Xu, Y. Y. Structure Formation and Characterization of PVDF Hollow Fiber Membrane Prepared via TIPS with Diluent Mixture. *J. Membr. Sci.* **2008**, *319*, 264−270.
(37) Jung, J. T.; Kim, J. F.; Wang, H. H.; di Nicolo, E.; Drioli, E.; Lee, Y. M. Understanding the Non-Solvent Induced Phase Separation (NIPS) Effect during the Fabrication of Microporous PVDF Membranes via Thermally Induced Phase Separation (TIPS). *J. Membr. Sci.* **2016**, *514*, 250−263.
(38) Borhani Zarandi, M.; Amrollahi Bioki, H.; Mirbagheri, Z. A.; Tabbakh, F.; Mirjalili, G. Effect of Crystallinity and Irradiation on Thermal Properties and Specific Heat Capacity of LDPE & LDPE/EVA. *Appl. Radiat. Isot.* **2012**, *70*, 1−5.
(39) Shi, F.; Ma, J.; Wang, P.; Ma, Y. Effect of Quenching Temperatures on the Morphological and Crystalline Properties of PVDF and PVDF−TiO2 Hybrid Membranes. *J. Taiwan Inst. Chem. Eng.* **2012**, *43*, 980−988.
(40) Wiener, O. Die Theorie Des Mischkorpers Fur Das Feld Der Stationaren Stromung. In *Abhandlungen der Sachsischen Gesellschaft der Akademischen Wissenschaften in Mathematik und Physik*; B. G. Teubner, 1912; Vol. 32, pp. 507−604.
(41) Fan, J.; Wang, L. Review of Heat Conduction in Nanofluids. *J. Heat Transfer* **2011**, *133*, No. 040801.
(42) Hashin, Z.; Shtrikman, S. A Variational Approach to the Theory of the Effective Magnetic Permeability of Multiphase Materials. *J. Appl. Phys.* **1962**, *33*, 3125−3131.
(43) Konuklu, Y.; Ostry, M.; Paksoy, H. O.; Charvat, P. Review on Using Microencapsulated Phase Change Materials (PCM) in Building Applications. *Energy Build.* **2015**, *106*, 134−155.
(44) He, F. R. Study on Manufacturing Technology of Phase Change Materials and Smart Thermo-Regulated Textiles. *Adv. Mater. Res.* **2013**, *821-822*, 130−138.
(45) Wu, H.; Zhang, X.; Wang, C.; Cao, R.; Yang, C. Experimental Study on Aerogel Passive Thermal Control Method for Cylindrical Lithium-Ion Batteries at Low Temperature. *Appl. Therm. Eng.* **2020**, *169*, No. 114946.
(46) *Phase Change Materials (Phasenwechselmaterial) Gütesicherung Quality Assurance RAL-GZ 896*.
(47) Islam, F.; Joannès, S.; Laiarinandrasana, L. Evaluation of Critical Parameters in Tensile Strength Measurement of Single Fibres. *J. Compos. Sci.* **2019**, *3*, 69.

https://doi.org/10.1021/acsomega.3c02318
ACS Omega 2023, 8, 26136−26146